Journal of Power Sources 221 (2013) 334–344

Contents lists available at SciVerse ScienceDirect

Journal of Power Sources

journal homepage: www.elsevier.com/locate/jpowsour

A distributed thermal model for a Li-ion electrode plate pair

Meng Guo, Ralph E. White*

Department of Chemical Engineering, University of South Carolina, Swearingen Engineering Center, 301 Main Street, Columbia, SC 29208, USA

HIGHLIGHTS

- A distributed thermal model for a lithium-ion electrode plate pair is developed.
- This model has multiple dimensions and multiple length scales.
- The model was developed by coupling the heat equation with a P2D electrochemical model.
- Reduced order model was also produced to significantly reduce the simulation time.

ARTICLE INFO

Article history:
Received 19 June 2012
Received in revised form
3 August 2012
Accepted 6 August 2012
Available online 11 August 2012

Keywords:
Lithium ion cell
Thermal modeling
Multi-scale
Model order reduction

ABSTRACT

This paper presents a distributed thermal model for a lithium-ion electrode plate pair used to predict the distributed electrical and thermal behavior of the electrode pair including tabs. Our model was developed by coupling the heat equation with a pseudo two dimensional (P2D) physics-based electrochemical model. The local heat generation rate is predicted by the P2D model at every node point in the 2D electrode pair. To reduce significantly the computation load of the model, a linear approximation method is introduced to decouple the electrochemical model from the heat equation with a very slight loss in accuracy.

1. Introduction

Currently, large-format Li-ion cells are widely used in the hybrid electrical vehicles (HEV), and these cells are often operated at very harsh electrical and thermal conditions such as the high and fast-changing current rates or extreme ambient temperatures. Under such conditions, the thermal and electrical behavior will be quite non-uniform through the cell volume [1–4]. Multi-scale and multi-dimensional (MSMD) modeling approaches have been proposed to simulate the distributed thermal, electrical, and chemical behavior of large format Li-ion cells [5–7]. The length scales of computational sub-domains in an MSMD model have typically three different levels: the microscopic, mesoscopic, and macroscopic [7,8]. Modeling in the microscopic scale generally focuses on the molecular-level quantum behavior, modeling in the mesoscopic scale specifically deals with the electrochemical processes and transport phenomena in the electrode coatings and the active material particles, and modeling in the macroscopic scale mainly describes the non-uniformity of the electric potential along the current collectors in electrode composites and the temperature throughout the cell volume [7,8]. In the fields of engineering and industry, models with mesoscopic-to-macroscopic length scales are more preferable for application; and among these models, the electrochemical-thermal (ECT) coupled models [1] are commonly used for the thermal management design and thermal runaway analysis.

Unfortunately, the physics-based MSMD models require a significant amount of computation time. The widely accepted physics-based model for Li-ion cells, Newman's pseudo-2D (P2D) porous electrode model [9–11], involves a large non-linear DAE system in the mesoscopic scale. Although various model order reduction techniques have been suggested to simplify the Newman's P2D model and reduce the computation time for a MSMD model [12–17], the reduced order models (ROM) still have disadvantages in terms of the accuracy for high current rates simulation. For example, the SVM model, which was derived by Smith et al. [12,13] and employed in the MSMD model by G-H Kim et al. [7] show poor agreement with the full-order model in the voltage response when the current rate exceeds 5C. Therefore, the goal of

* Corresponding author. Tel.: +1 803 777 3270; fax: +1 803 777 0973.
E-mail address: white@cec.sc.edu (R.E. White).

0378-7753/$ – see front matter © 2012 Elsevier B.V. All rights reserved.
http://dx.doi.org/10.1016/j.jpowsour.2012.08.012

good time-efficiency in simulation as well as sufficient accuracy in predictions is a great challenge for researchers in the MSMD modeling for the Li-ion cells.

In this work, we present our full physics-based (P2D) MSMD model and an associated ROM for a Li-ion electrode pair with planar electrode. We derived our ROM by segregating the mesoscopic and the macroscopic sub-domains, that is, we decoupled the Newman's P2D model from the charge balance in the current collectors and the energy balance in the cell volume. Significant improvements in the simulation speed were achieved through our model order reduction approach. To ensure that our ROM also maintains sufficient accuracy in predictions, extensive model-to-model validations were made between the ROM and the full-order full-distribution model.

2. Mathematical model

In this part of work, the model developments and simulation case studies are based on one single electrode plate pair; and in the future, the model will be extended to cell stacks that include multiple electrode pairs.

2.1. The modeling scales and sub-domains

The planar electrode plate pair of the Li-ion cell can be divided into several computational sub-domains in terms of length scales (see Fig. 1). As shown in Fig. 1, the thickness of electrode pair (the x dimension) and the radius of particles (the r dimension) are much smaller than the length and width of the electrode pair (the X and Y dimensions). Therefore, in our model, the macroscopic sub-domains include the electroactive part of the electrode plate pair (the cell sub-domain) and the two electrode tabs; the mesoscopic sub-domains include the porous electrode coatings and separator (the porous electrode sub-domain), and the active material particles (the particle-sub-domain). According to a dimensional analysis, the temperature and the electrical potential of each current collector can be considered to be distributed only in the two macroscopic (X and Y) dimensions; the mass and charge transport in the electrolyte and the solid phase in the porous electrode sub-domain follow the mesoscopic (x) dimension; the mass balance in the particle sub-domain is described by another mesoscopic dimension, the r dimension. Table 1 summarizes the dependent variables to be solved in the different sub-domains.

2.2. The models in the macroscopic sub-domains

2.2.1. The current collector charge balance

A schematic for the planar and transverse current density distribution on the two current collectors including the tabs is presented in Fig. 2. The governing equations for the charge balance in the current collectors of the cell sub-domain are as follow:

$$\sigma_{\mathrm{cc},j}\frac{\partial^2\Phi_j}{\partial X^2}+\sigma_{\mathrm{cc},j}\frac{\partial^2\Phi_j}{\partial Y^2}+\frac{i_{N,j}}{\delta_j}=0 \quad (j=p,n) \tag{1}$$

where Φ_j is the potential in the current collector of electrode j, $\sigma_{\mathrm{cc},j}$ is the electrical conductivity of current collector, δ_j is the thickness of current collector, and $i_{N,j}$ is the normal inward current density through the coating/current-collector interfaces. In the tab sub-domains, there is no transverse current, and the charge balance equations are:

$$\sigma_{\mathrm{cc},j}\frac{\partial^2\Phi_j}{\partial X^2}+\sigma_{\mathrm{cc},j}\frac{\partial^2\Phi_j}{\partial Y^2}=0 \quad (j=p,n) \tag{2}$$

The boundary conditions (see Fig. 2) at the tops of electrode tabs are:

$$n\cdot(-\sigma_{\mathrm{cc},j}\nabla\Phi_j)=i_{\mathrm{app},j} \tag{3}$$

where n is the unit normal vector pointing out of the boundary, and $i_{\mathrm{app},j}$ is the applied outward current density based on the cross section at the top of each electrode tab.

2.2.2. The energy balance

The equation for the energy balance in the cell and tab sub-domains is:

$$\rho C_P\frac{\partial T}{\partial t}=k_{X-Y}\frac{\partial^2 T}{\partial X^2}+k_{X-Y}\frac{\partial^2 T}{\partial Y^2}+Q-Q_{\mathrm{Trans}} \tag{4}$$

where T is the temperature of the sub-domain, ρ is the density of the electrode plate pair, C_P is the specific heat capacity of the electrode plate pair, k_{X-Y} is the thermal conductivity of the

Table 1
The dependent variables in different sub-domains.

Length scale	Sub-domain	Dependent variable name	Symbol	Independent variables
Macroscopic	Cell and tabs	Temperature (K)	T	t,X,Y
		Current collector potential (V)	$\Phi_j(j=p,n)$	t,X,Y
Mesoscopic	Porous electrode	Li concentration in electrolyte (mol m^{-3})	c_e	t,x,X,Y
		Potential in solution phase (V)	ϕ_2	t,x,X,Y
		Potential in solid phase (V)	ϕ_1	t,x,X,Y
		Surface reaction rate (mol m^{-2} s^{-1})	$J_j(j=p,n)$	t,x,X,Y
	Particle	Li concentration in solid phase (mol m^{-3})	$c_{s,j}(j=p,n)$	t,r,x,X,Y

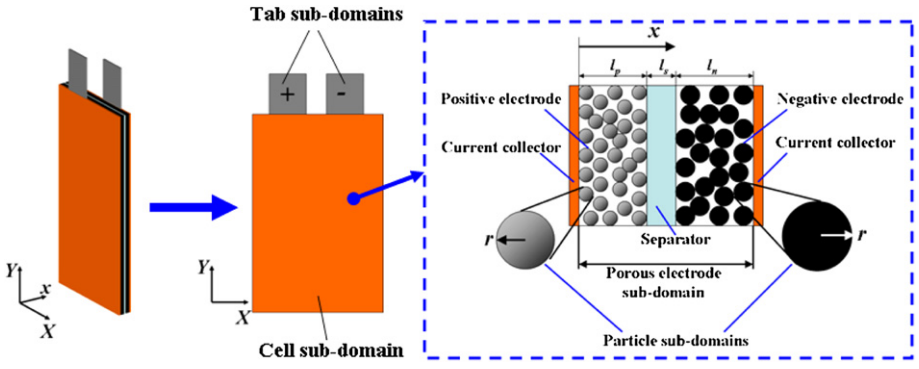

Fig. 1. The computational sub-domains in an electrode plate pair.

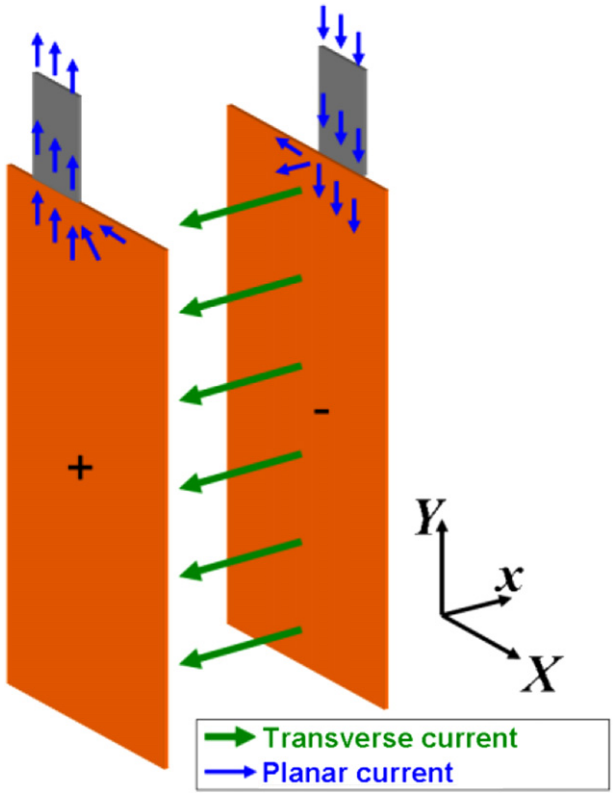

Fig. 2. Schematic for the charge balance (current flow) in current collectors and tabs (discharge process).

electrode plate pair in the X–Y plane, Q is the volumetric heat source, and Q_{Trans} is the heat transfer rate between the electrode plate pair and the surroundings.

In Equation (4), the heat source term Q is divided into three parts:

$$Q = \varepsilon_e Q_{\text{ECh}} + \varepsilon_{\text{cc},p} Q_{J,p} + \varepsilon_{\text{cc},p} Q_{J,n} \tag{5}$$

where Q_{ECh} is the electrochemical heat generated in the porous electrode sub-domain, $Q_{J,p}$ and $Q_{J,n}$ are the Joule heating rates in the current collectors and tabs, ε_e, $\varepsilon_{\text{cc},p}$, and $\varepsilon_{\text{cc},n}$ are, respectively, the volume ratio factors for the porous electrode, positive electrode current collector, and negative electrode current collector. The expressions for ε_e, $\varepsilon_{\text{cc},p}$, and $\varepsilon_{\text{cc},n}$ in different sub-domains are listed in Table 2. Fig. 3 shows the thermal conditions for a unit cross area (in X–Y plane) of electrode plate pair. The planar current densities along the X–Y plane are expressed as:

$$i_{X,j} = -\sigma_{\text{cc},j} \frac{\partial \Phi_j}{\partial X} \quad \text{and} \quad i_{Y,j} = -\sigma_{\text{cc},j} \frac{\partial \Phi_j}{\partial Y} \quad (j = p, n) \tag{6}$$

The Joule heating rates in the Equation (5) are expressed as:

Table 2
The expressions for the volume fraction and the thickness.

Parameter	Sub-domain		
	Tab of positive electrode	Tab of negative electrode	Cell
ε_e	0	0	$\frac{l_p + l_s + l_n}{\delta_p + l_p + l_s + l_n + \delta_n}$
$\varepsilon_{\text{cc},p}$	1	0	$\frac{\delta_p}{\delta_p + l_p + l_s + l_n + \delta_n}$
$\varepsilon_{\text{cc},n}$	0	1	$\frac{\delta_n}{\delta_p + l_p + l_s + l_n + \delta_n}$
d	δ_p	δ_n	$\delta_p + l_p + l_s + l_n + \delta_n$

$$Q_{J,j} = \frac{1}{\sigma_{\text{cc},j}} \left(i_{X,j}^2 + i_{Y,j}^2 \right) \tag{7}$$

If the transverse heat flux follows the Newton's law of cooling, the term Q_{Trans} is expressed as:

$$Q_{\text{Trans}} = \frac{h(T - T_{\text{amb}})}{0.5d} \tag{8}$$

where h is the heat transfer coefficient, d is the distance between the two planar heat transfer surfaces, and T_{amb} is the ambient temperature. The expressions for d in the different sub-domains are listed in the bottom row of Table 2

2.3. The models in the mesoscopic sub-domain

The electrochemical processes and transport phenomena in the porous electrode and particles are described by the pseudo-2D model derived by Doyle et al. [9].

2.3.1. The solution phase mass transfer

The governing equation for diffusion of lithium ion in the solution phase is

$$\varepsilon_j \frac{\partial c_e}{\partial t} = \frac{\partial}{\partial x} \left(D_{2,\text{eff}} \frac{\partial c_e}{\partial x} \right) + a_j \left(1 - t^+ \right) J_j \quad j = p, n \tag{9}$$

Insulation boundary conditions are assumed at the interface between the coatings and the current collectors:

$$\left. \frac{\partial c_e}{\partial x} \right|_{x=0} = 0 \text{ and } \left. \frac{\partial c_e}{\partial x} \right|_{x=l_p+l_s+l_n} = 0 \tag{10}$$

where a_j is the specific surface area of porous electrode, c_e is the lithium ion concentration in the solution phase, $D_{2,\text{eff}}$ is the effective diffusion coefficient of solution phase, t^+ is the transference number, J_j is the rate of electrochemical reaction at the solid/solution surface, and ε_j is the porosity of porous electrode j. The second term on the right-hand side (the source term) of Equation (9) is zero in the separator since there is no reaction in that region, and the porosity ε_j ($j = p,n$) on the left-hand-side is then replaced by the separator porosity ε_s. The effective diffusion coefficient in solution phase is calculated as:

$$D_{2,\text{eff}} = D_{e,\text{bulk}} \varepsilon_j^{\beta_j} \quad j = p, s, n \tag{11}$$

where $D_{e,\text{bulk}}$ is the diffusion coefficient in bulk solution phase (see Appendix A), and β_j is the Bruggeman factor.

2.3.2. The solution phase charge balance

The solution phase current density is defined as:

$$i_2 = -\kappa_{\text{eff}} \frac{\partial \phi_2}{\partial x} - \frac{2RT}{F} \left(1 - t^+ \right) \left(1 + \frac{d \ln f_{\pm}}{d \ln c_e} \right) \frac{\partial \ln c_e}{\partial x} \tag{12}$$

where κ_{eff} is the ionic effective electrical conductivity of solution phase, R is the universal gas constant, F is the Faraday's constant, and $f_{\pm}$ is the activity coefficient of solution phase. The effective electrical conductivity of solution phase is calculated as:

$$\kappa_{\text{eff}} = \kappa_{\text{bulk}} \varepsilon_j^{\beta_j} \quad j = p, s, n \tag{13}$$

where κ_{bulk} is the electrical conductivity in bulk solution (see Appendix A). The conservation of charge in the solution phase is described as

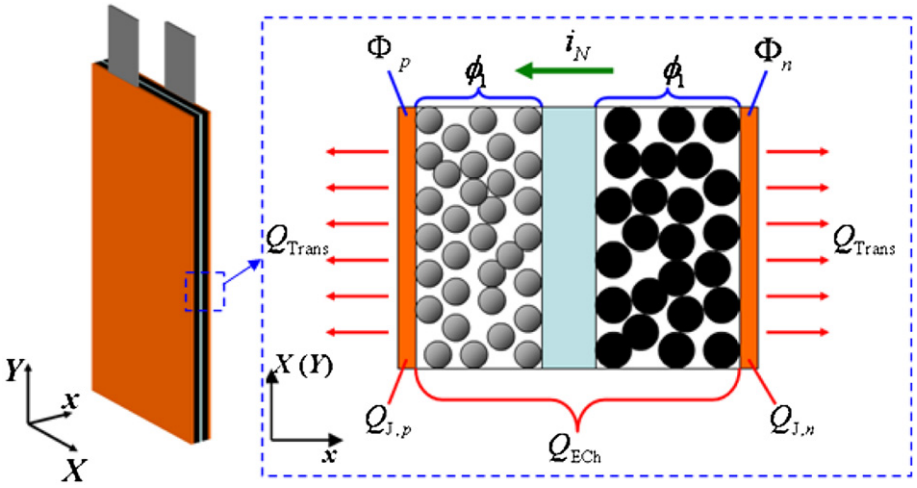

Fig. 3. Schematic for the thermal conditions of cell.

$$\frac{\partial i_2}{\partial x} = a_j F J_j \quad j = p, n \tag{14}$$

with boundary conditions

$$i_2|_{x=0} = 0 \text{ and } i_2|_{x=l_n+l_s+l_p} = 0 \tag{15}$$

2.3.3. The solid phase charge balance

The solid phase current density is defined as:

$$i_1 = -\sigma_{j,\text{eff}} \frac{\partial \phi_1}{\partial x} \quad j = p, n \tag{16}$$

The effective electrical conductivity of solid phase $\sigma_{j,\text{eff}}$ is defined as:

$$\sigma_{j,\text{eff}} = \sigma_j \varepsilon_{s,j}^{\beta_j} \tag{17}$$

where σ_j is the electrical conductivity of pure active material for electrode j, and $\varepsilon_{s,j}$ is the volume fraction of active material in the electrode j. There is no solid phase current in the separator region. The conservation of charge in solid phase charge is described as:

$$\frac{\partial i_1}{\partial x} = -a_j F J_j \quad j = p, n \tag{18}$$

with boundary conditions:

$$\phi_1|_{x=0} = \Phi_p, \; i_1|_{x=l_p} = 0, \; i_1|_{x=l_p+l_s} = 0, \text{ and } \phi_1|_{x=l_p+l_s+l_n} = \Phi_n \tag{19}$$

Equation (19) suggests that the solid phase charge balance in the porous electrode sub-domain is coupled to the macroscopic cell sub-domain at the two boundaries of x dimension where the potential of coatings equals to the potential of current collector. It can be derived that the boundary values for the solid phase current density at the two current collectors are equal:

$$i_1|_{x=l_p+l_s+l_n} = i_1|_{x=0} \tag{20}$$

The terms $i_{N,j}$ (where $j = p,n$) in the cell sub-domain charge balance Equation (1) are coupled to the porous electrode sub-domain through the following correlations

$$i_1|_{x=0} = -i_{N,p} \tag{21}$$

$$i_1|_{x=l_p+l_s+l_n} = i_{N,n} \tag{22}$$

In this work, the one-direction transverse current density is defined as:

$$i_N = i_{N,p} = -i_{N,n} \tag{23}$$

2.3.4. The electrochemical reaction kinetics

The surface electrochemical reactions for lithium intercalation/deintercalation are expressed as follow:

$$\text{Li} - \theta_s \rightleftarrows \text{Li}^+ + e^- + \theta_s \tag{24}$$

where θ_s represents a vacant host on the solid particle surface. The rate for this reaction is described by the Butler–Volmer equation

$$J_j = k_{r,j} c_e^{0.5} \left(c_{s,j,\max} - c_{s,j,\text{surf}}\right)^{0.5} c_{s,j,\text{surf}}^{0.5} \left[\exp\left(\frac{0.5F}{RT}\eta_j\right) - \exp\left(-\frac{0.5F}{RT}\eta_j\right)\right] \tag{25}$$

where $k_{r,j}$ is the reaction rate constant, and the electrolyte concentration in solution phase, $c_{s,j,\text{surf}}$ is the concentration of lithium at the surface of solid phase particles, and $c_{s,j,\max}$ is the maximum lithium concentration in the solid phase particles. The electrode overpotential η_j is defined as:

$$\eta_j = \phi_1 - \phi_2 - U_j \quad j = p, n \tag{26}$$

where U_j is the open circuit potential which depends on both the surface state-of-charge and temperature (see Appendix A).

2.3.5. The electrochemical heat source

The electrochemical heat source term Q_{ECh} in Equation (5) is expressed by the integrating the addition of volumetric reversible heat and irreversible heat along thickness of porous electrode sub-domain.

$$Q_{\text{ECh}} = \frac{1}{L_p + L_s + L_n} \int_0^{L_p+L_s+L_n} \left(q'_{\text{rev}} + q'_{\text{irrev}}\right) dx \tag{27}$$

where q'_{rev} and q'_{irrev}, respectively, denote the local reversible heat and irreversible heat along the dimension x, and are defined as follow:

$$q'_{\text{rev}} = a_j F J_j T \frac{\partial U_j}{\partial T} \quad j = p,n \tag{28}$$

$$q'_{\text{irrev}} = -i_1 \frac{\partial \phi_1}{\partial x} - i_2 \cdot \frac{\partial \phi_2}{\partial x} + a_j F J_j \eta_j \quad j = p,n \tag{29}$$

As the overpotential is defined as:

$$\eta_j = \phi_1 - \phi_2 - U_j \quad j = p,n \tag{30}$$

Equation (29) can be rewritten as:

$$q'_{\text{irrev}} = -i_1 \frac{\partial \phi_1}{\partial x} - i_2 \cdot \frac{\partial \phi_2}{\partial x} + a_j F J_j \phi_1 - a_j F J_j \phi_2 - a_j F J_j U_j \tag{31}$$

Substitute Equations (14) and (18) into Equation (31) and obtain:

$$q'_{\text{irrev}} = -i_1 \frac{\partial \phi_1}{\partial x} - i_2 \cdot \frac{\partial \phi_2}{\partial x} - \frac{\partial i_1}{\partial x}\phi_1 - \frac{\partial i_2}{\partial x}\phi_2 - a_j F J_j U_j \tag{32}$$

Equation (32) can be rewritten as:

$$q'_{\text{irrev}} = -\frac{\partial (i_1 \phi_1 + i_2 \phi_2)}{\partial x} - a_j F J_j U_j \tag{33}$$

Integrate the right-hand-side of Equation (33) from 0 to $l_p + l_s + l_n$ along the x-dimension

$$\int_0^{l_p+l_s+l_n} q'_{\text{irrev}} dx = -(i_1\phi_1 + i_2\phi_2)\big|_{x=0}^{x=l_p+l_s+l_n} - \int_0^{l_p+l_s+l_n} a_j F J_j U_j dx \tag{34}$$

According to the boundary conditions of charge balance in the solution phase and solid phase presented in Equations (15) and (19), and applying the correlations shown in Equations (20)–(23), Equation (34) can be simplified to

$$\int_0^{l_p+l_s+l_n} q'_{\text{irrev}} dx = -i_N(\Phi_p - \Phi_n) - \int_0^{l_p+l_s+l_n} a_j F J_j U_j dx \tag{35}$$

Substitute Equations (28) and (35) into (27), so that the heat source term can be expressed as

$$Q_{\text{ECh}} = \frac{-i_N(\Phi_p - \Phi_n) + \int_0^{l_p+l_s+l_n} a_j F J_j \left(T \frac{\partial U_j}{\partial T} - U_j \right) dx}{L_p + L_s + L_n} \tag{36}$$

The temperature-dependent open circuit potential is expressed in Taylor's expansion:

$$U_j = U_{j,\text{ref}} + \frac{\partial U_j}{\partial T}\left(T - T_{\text{ref}}\right) \tag{37}$$

where T_{ref} is the reference temperature and $U_{j,\text{ref}}$ is the open circuit potential at reference temperature. Substitute Equation (37) into Equation (36) and obtain

$$Q_{\text{ECh}} = \frac{-i_N(\Phi_p - \Phi_n) + \int_0^{l_p+l_s+l_n} a_j F J_j \left(T_{\text{ref}} \frac{\partial U_j}{\partial T} - U_{j,\text{ref}} \right) dx}{L_p + L_s + L_n} \tag{38}$$

Let

$$W_E = \frac{-i_N(\Phi_p - \Phi_n)}{L_p + L_s + L_n} \tag{39}$$

and

$$Q_H = \frac{1}{L_p + L_s + L_n} \int_0^{l_p+l_s+l_n} a_j F J_j \left(T_{\text{ref}} \frac{\partial U_j}{\partial T} - U_{j,\text{ref}} \right) dx \tag{40}$$

And the heat source term can be expressed as the addition of W_E and Q_H

$$Q_{\text{ECh}} = W_E + Q_H \tag{41}$$

where W_E describes the local electrical work on the porous electrode and Q_H describes the local reaction enthalpy change throughout the porous electrode sub-domain. According to the Thermal Equations (4) and (5), the energy balance in the cell sub-domain is coupled to the porous electrode sub-domain through Q_{ECh}. For the high rate (i.e. 5C) results presented in this paper, we have chosen to neglect the entropy term, $\partial U_j/\partial T$, in Equation (40). This term should be included for low rate operations.

2.3.6. The solid phase diffusion

The diffusion of lithium in the solid phase follows Fick's second law in a spherical coordinate system, and the governing equation is:

$$\frac{\partial c_{s,j}}{\partial t} = D_{s,j} \frac{1}{r^2} \frac{\partial}{\partial r}\left(r^2 \frac{\partial c_{s,j}}{\partial r} \right) \quad (j = p,n) \tag{42}$$

where $c_{s,j}$ is the concentration of lithium in the solid phase particles, $D_{s,j}$ is the solid phase diffusion coefficient of lithium. The boundary conditions for the solid phase diffusion are:

$$-D_{s,j} \frac{\partial c_{s,j}}{\partial r}\bigg|_{r=0} = 0 \tag{43}$$

$$-D_{s,j} \frac{\partial c_{s,j}}{\partial r}\bigg|_{r=R_{s,j}} = J_j \tag{44}$$

where $R_{s,j}$ is the radius of particle. The state of charge for electrode, θ_j, is defined as:

$$\theta_j = \frac{c_{s,j}}{c_{s,j,\max}} \tag{45}$$

In Equation (26), the open circuit potential of electrode, U_j, is dependent on state of charge θ_j through the correlations presented in Appendix A. The surface lithium concentration $c_{s,j,\text{surf}}$ is defined as:

$$c_{s,j,\text{surf}} = c_{s,j}\big|_{r=R_{s,j}} \tag{46}$$

According to Equations (25), (44)–(46), the particle sub-domain and porous electrode sub-domain are coupled through $c_{s,j,\text{surf}}$ and J_j.

2.4. The temperature dependency of parameters

The transport and kinetic parameters of cell materials are affected by temperature. The diffusion coefficient and ionic electrical

Table 3
Parameter values for LG pouch cell.

Sub-domain	Parameter	Value		
		Positive electrode		Negative electrode
Particle	Maximum Li capacity $c_{s,j,\max}$ (mol m^{-3})	49,000		28,700
	Radius of particle $R_{s,j}$ (m)	5.0×10^{-6}		12.5×10^{-6}
	Reference particle diffusion coefficient $D_{s,j,\mathrm{ref}}$ (m^2 s^{-1})	3.0×10^{-15}		9.0×10^{-14}
	Activation energy for particle diffusion $\mathrm{Ea}_{\mathrm{di},j}$ (J mol^{-1})	4.0×10^{3}		2.0×10^{4}
		Positive electrode	Separator	Negative electrode
Porous electrode	Average electrolyte concentration $\bar{c}_e$ (mol m^{-3})		1200	
	Activity coefficient of solution phase $f_{\pm}$		0	
	Thickness l_p l_s l_n (m)	50×10^{-6}	25×10^{-6}	70×10^{-6}
	Bruggeman factor β_j	2.0	2.0	2.0
	Porosity ε_p ε_s ε_n	0.4	0.4	0.4
	Volume fraction of active material $\varepsilon_{s,j}$	0.41		0.51
	Specific surface area a_p a_n (m^2 m^{-3})	2.66×10^{5}		1.02×10^{5}
	Solid electronic capacity σ_p σ_n (S m^{-1})	10		100
	Reference reaction rate constant $k_{r,p,\mathrm{ref}}$ $k_{r,n,\mathrm{ref}}$ (m$^{2.5}$ mol$^{-0.5}$ s^{-1})	4.966×10^{-11}		7.773×10^{-10}
	Activation energy for reaction $\mathrm{Ea}_{\mathrm{re},p}$ $\mathrm{Ea}_{\mathrm{re},n}$ (J mol^{-1})	3.0×10^{4}		3.0×10^{4}
	The universal gas constant R (J mol^{-1} K^{-1})		8.314	
	The Faraday constant F (C mol^{-1})		96,487	
		Positive electrode		Negative electrode
Cell	Current collector thickness δ_j (m)	10×10^{-6}		15×10^{-6}
	Current collector electronic conductivity $\sigma_{\mathrm{cc},j}$ (S m^{-1})	37.8×10^{6}		59.6×10^{6}
	Volumetric heat capacity ρC_P (J K^{-1} m^{-3})		2.575×10^{6}	
	Planar thermal conductivity k_{X-Y} (W K^{-1} m^{-1})		27	
		Positive electrode		Negative electrode
Tabs	Current collector thickness δ_j (m)	10×10^{-6}		15×10^{-6}
	Current collector electronic conductivity $\sigma_{\mathrm{cc},j}$ (S m^{-1})	37.8×10^{6}		59.6×10^{6}
	Volumetric heat capacity ρC_P (J K^{-1} m^{-3})	2.42×10^{6}		3.41×10^{6}
	Planar thermal conductivity k_{X-Y} (W K^{-1} m^{-1})	237		401

conductivity of solution phase are dependent on temperature and electrolyte concentration through the empirical correlations presented in Appendix A. The diffusion coefficients of solid phase and the rate constants for the intercalate/deintercalate reactions are dependent on temperature through Arrhenius' equations:

$$D_{s,j} = D_{s,j,\mathrm{ref}} \exp\left[-\frac{\mathrm{Ea}_{\mathrm{di},j}}{R}\left(\frac{1}{T}-\frac{1}{T_{\mathrm{ref}}}\right)\right] \tag{47}$$

$$k_{r,j} = k_{r,j,\mathrm{ref}} \exp\left[-\frac{\mathrm{Ea}_{\mathrm{re},j}}{R}\left(\frac{1}{T}-\frac{1}{T_{\mathrm{ref}}}\right)\right] \tag{48}$$

where $D_{s,j,\mathrm{ref}}$ and $k_{rj,\mathrm{ref}}$ are respectively the solid phase diffusion coefficients and reaction rate constants at reference temperature T_{ref}, and $\mathrm{Ea}_{\mathrm{di},j}$ and $\mathrm{Ea}_{\mathrm{re},j}$ are, respectively, the activation energy for solid phase diffusion and intercalate/deintercalate reactions (see Table 3).

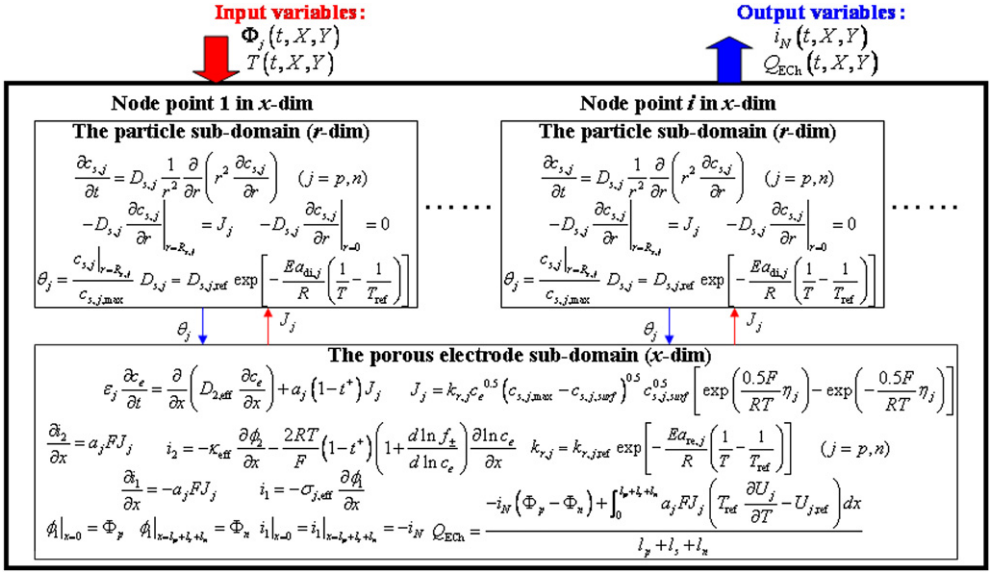

Fig. 4. The pseudo-2D model expressed as control block.

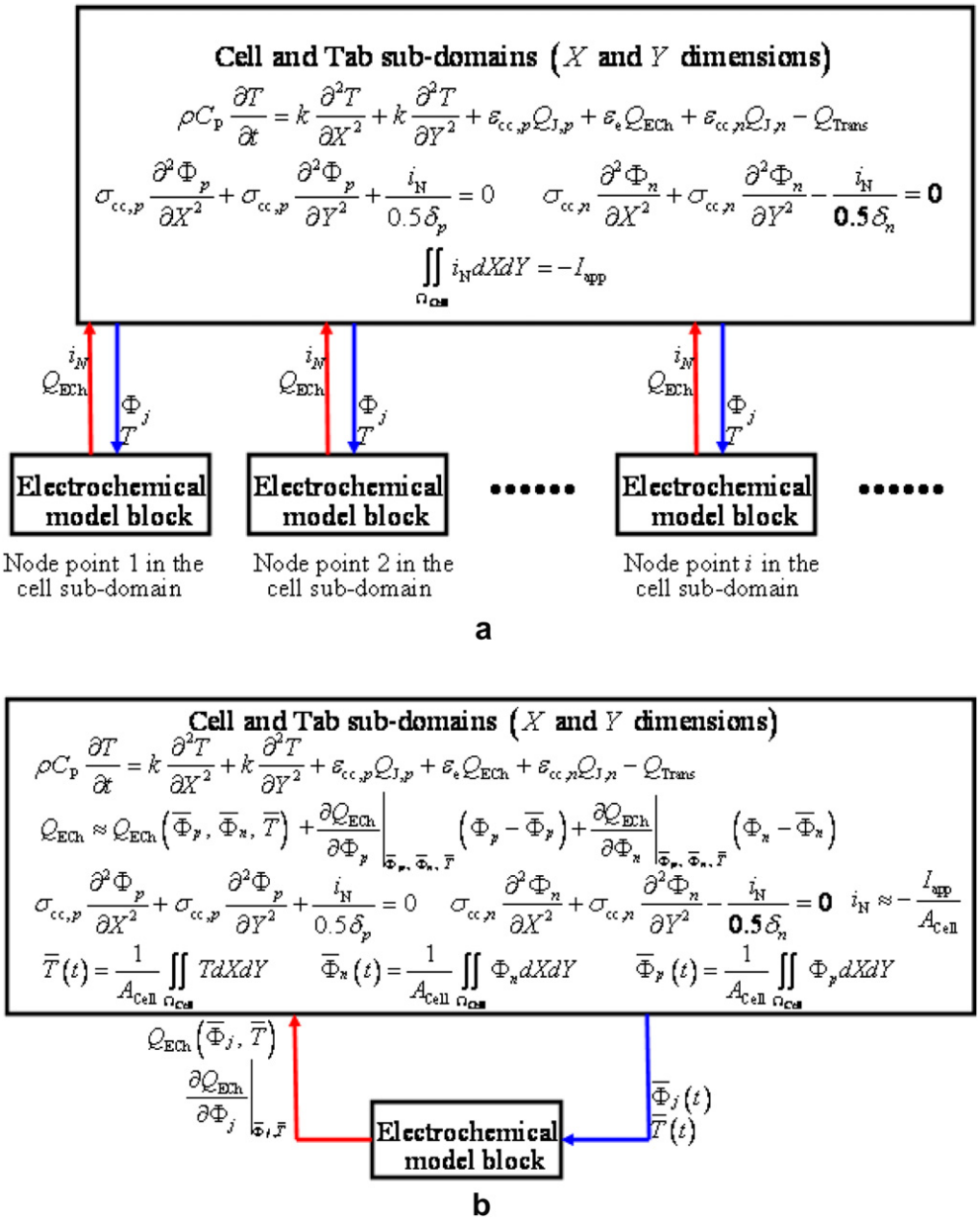

Fig. 5. The two types of model-coupling approaches: (a) the full-distribution model, (b) the linear model.

2.5. The electrical limiting condition

According to Equation (3), there is no imposed boundary condition for the current collector charge balance; therefore, two additional equations are needed to determine the unique values for the electrical potentials of the current collectors. The first equation is obtained by setting the potential at the top-center of negative electrode tab to be zero, and the second equation is the electrical limiting equation that the integration of transverse current density through the cell sub-domain equals the total applied current on the electrode pair:

$$\int\int_{\Omega_{Cell}} i_N dXdY = -I_{app} \tag{49}$$

where I_{app} is the total applied current passing through the electrode pair and is defined as negative for discharge.

2.6. The coupling of models of different length scales

In this work, the Newman's pseudo-2D model in the mesoscopic dimensions was expressed as a control block as presented in Fig. 4. The inputs for the control block are the temperature T which affects certain transport and kinetic processes, and the current collector potentials Φ_j ($j = p,n$) which act as boundary values for the solid-phase charge balance at the interfaces between coatings and current collectors. The outputs from the control block are the transverse current density i_N and the electrochemical heat source Q_{ECh}. As the input variables are distributed with the macroscopic dimensions, the pseudo-2D control block has to be solved at every node point of the cell sub-domain and then return the local electrical and thermal outputs (Fig. 5(a)) to the charge balance Equation (1) and the energy balance Equation (4). In this work, this model coupling approach as described in Fig. 5 is named as the full-

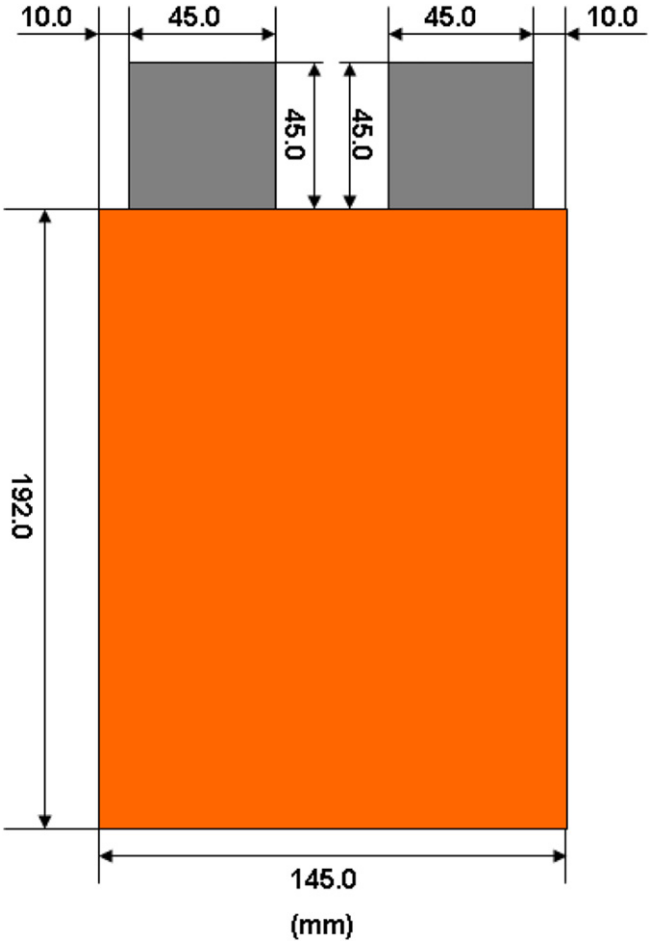

Fig. 6. The dimensions of electrode in the LG pouch cell.

distribution model. The disadvantage of full-distribution model is that a very huge non-linear differential–algebraic equation (DAE) system is to be solved in simulations. Therefore, the full-distribution model is very time-consuming although it accurately describes the non-uniformity of cell's thermal and electrical behaviors.

Alternatively, in our work, a simplification method is proposed to produce our ROM and reduce the simulation time and memory requirements. Instead of using the reduced-order model to replace pseudo-2D model, our simplification method focuses on the segregation of sub-domains. As shown in (Fig. 5b), the distributed input variables for the pseudo-2D control block are replaced by the volume-average of those variables through the cell sub-domain; the electrochemical heat source returned to the macroscopic sub-domains are approximated linearly through the following Taylor's expansion:

$$Q_{\mathrm{ECh}} \approx Q_{\mathrm{ECh}}\left(\overline{\Phi}_p,\ \overline{\Phi}_n,\ \overline{T}\right) + \left.\frac{\partial Q_{\mathrm{ECh}}}{\partial \Phi_p}\right|_{\overline{\Phi}_p,\ \overline{\Phi}_n,\ \overline{T}} \left(\Phi_p - \overline{\Phi}_p\right) + \left.\frac{\partial Q_{\mathrm{ECh}}}{\partial \Phi_n}\right|_{\overline{\Phi}_p,\ \overline{\Phi}_n,\ \overline{T}} \left(\Phi_n - \overline{\Phi}_n\right) \tag{50}$$

Equation (50) was derived by assuming that the spatial variation of current collector potential is the major reason for the distribution of the electrochemical heat source. This assumption can be verified by Equation (38)–(41), Equation (39) suggests that the electrical work on the porous electrode is almost a linear function of the current collector potentials, where the derivatives of W_E to Φ_j are:

$$\frac{\partial W_E}{\partial \Phi_p} = -\frac{i_N}{L_p + L_s + L_n} \quad \text{and} \quad \frac{\partial W_E}{\partial \Phi_n} = \frac{i_N}{L_p + L_s + L_n} \tag{51}$$

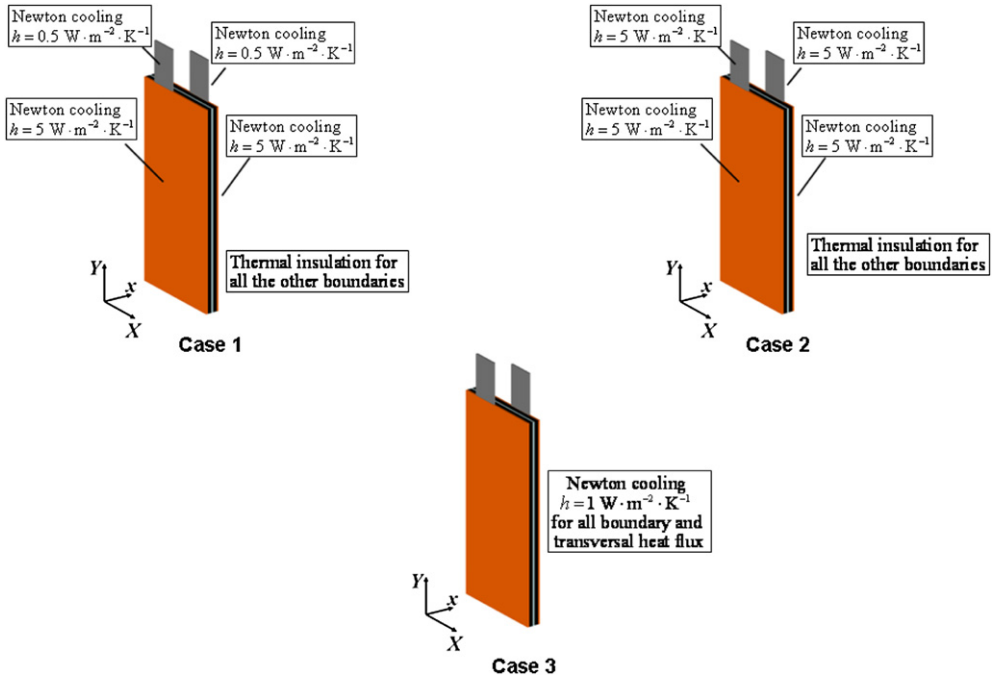

Fig. 7. The boundary and transversal thermal condition settings for different cases.

Table 4
The computation time for case studies.

Model type	Number of equations	Simulation time		
		Case 1	Case 2	Case 3
Full-distribution	7576	5510 s	6371 s	5498 s
Linear	361	6.26 s	6.33 s	6.60 s

Equation (40) suggests that the reaction enthalpy Q_H only depends on the entropy change and the electrode open circuit potential at the reference temperature, and the distributions of these variables in the macroscopic dimensions are neglected. The transverse current returned from the pseudo-2D control block was replaced by the volume-average value in the cell sub-domain:

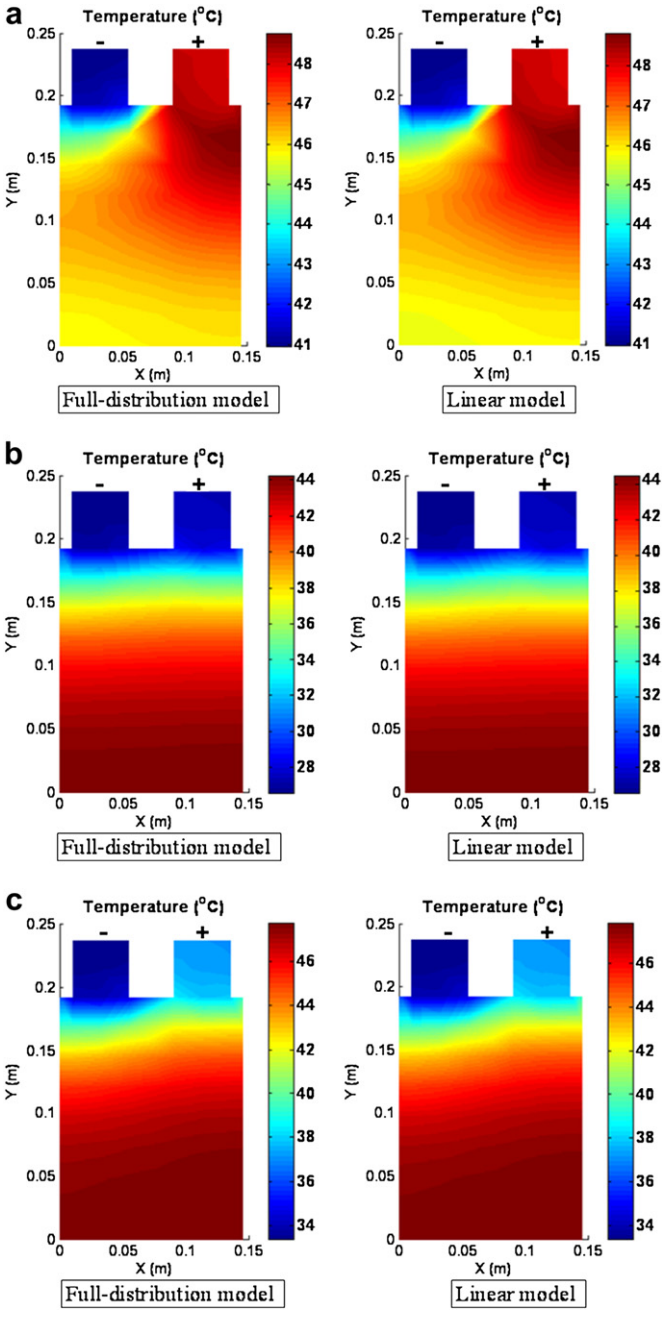

Fig. 8. The simulated end-of-discharge temperature profiles for different cases: (a) case 1, (b) case 2, (c) case 3.

$$i_N \approx -\frac{I_{app}}{A_{Cell}} \tag{52}$$

where A_{Cell} is the area of the cell sub-domain. In this work, this approximated model coupling approach is called as the linear model; and through this method, the pseudo-2D electrochemical model was only evaluated once at the average temperature and potential in the cell sub-domain, time and computer memory was significantly saved.

3. Results and discussion

In proposing the linear approximation approach, our concerns include how much computation time can be saved by decoupling the sub-domains and how well the linear model can agree with the full-distribution model. Case studies were also made in this work to analyze the distribution of heat source and planar/transverse current density. As our model was just based on one single planar electrode pair, the model-to-data validations will be made in future work until the model is extended to the cell stacks with multiple electrode pairs.

In our work, the model was based on the electrode plate pair of LG pouch cell (see Kim et al. [7]), the electrode dimensions are presented in Fig. 6. The physical and chemical properties of the electrodes are presented in Table 3, where the active materials for the positive and negative electrodes are, respectively, $LiNi_{0.8}Co_{0.15}Al_{0.05}O_2$ (NCA) andLi_xC_6. This model was solved using the Galerkin's finite element method; the setting of geometry, the meshing of sub-domains, the solving of DAE system, and the post-processing of results, were all performed by MATLAB.

The comparisons between the linear model and the full-distribution model were made by simulating the 5*C* (where $C = 0.4186$ A for one electrode pair) discharge of electrode with three different boundary and transversal thermal conditions as presented in Fig. 7. The initial state-of-charge (SOC) is 0.41 for positive electrode and 0.63 for negative electrode, the cut-off voltage is 3 V, and both the ambient temperature and the initial temperature of cell are 25 °C. The computation time that the linear model and the full-distribution model take for each simulation are listed in Table 4, and the linear model is faster than the full-distribution model by about 900 times.

The temperature profiles at the end of 5*C* discharge simulated by the linear and the full-distribution models for the three different cases are presented in Fig. 8(a)–(c). According to these plots, the maximum temperature difference between the hottest and the coldest spots of the cell is 16.5 °C (in case 2); and in these cases, the linear model shows excellent agreements with the full-distribution model. The results in Fig. 8 also show that the temperature of the positive electrode tab is always higher that that of the negative electrode tab, the reason is that the current collector of positive electrode which is made by the aluminum foil has larger electrical resistivity than the current collector of negative electrode which is made by the copper foil, and thus more Joule heat is generated on the positive electrode than on the negative electrode. In Fig. 8(b) and (c) (case 2 and case 3), the temperature of the two electrode tabs is lower than that of the cell sandwich when transversal and boundary thermal conditions are same for both cell and tabs. The reason is that the tabs have much smaller thickness than the cell sandwich; and according to Equation (8), the transversal heat transfer rate is inversely proportional to the thickness, therefore the heat dissipates much faster on the tabs than on the surface of cell sandwich. In Fig. 8(a) (case 1) where the heat transfer coefficient on the tabs is smaller than that on the cell sandwich, the negative electrode tab is the coldest part; the hottest spot locates in the top-left part of the cell sub-domain which is close to the tab of

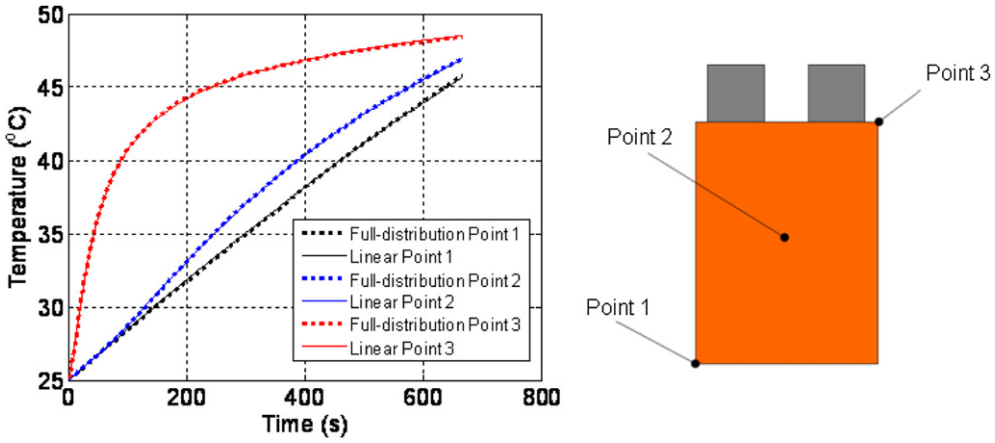

Fig. 9. The temperature vs time plots at different points with thermal condition case 1.

the positive electrode; and temperature of other locations in the cell sun-domain lies between the temperature of the positive and negative electrode tabs. The plots for variation of temperature at three selected points with time during case 1 are presented in Fig. 9, and the linear model still agrees well with the full-distribution model. As shown in Fig. 9, the temperature of the upper point (point) rises rapidly at the beginning (0–100 s) and then the increase of temperature slows down; the temperature at lower points (points 1 and 2) just increases with nearly constant rates. The reason is that the temperature rise at point 3 is decelerated by the high thermal dissipation rate on the tab of positive electrode.

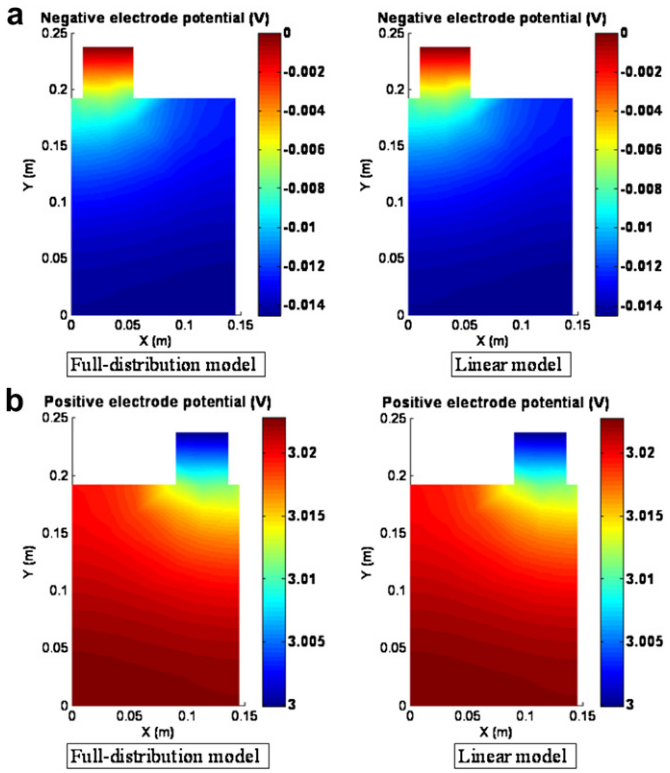

Fig. 10. The end-of-discharge potential profiles with thermal condition setting case 1.

The case studies above also show the great potential values for this model:

i) This model could be extended for life study by including capacity fade. The results suggest that the high non-uniformity of the cell thermal behavior could significantly affect the cycling life of Li-ion cells.
ii) This model could also be used for the design and optimization of cells and packs. For example, the results above show that the tab temperature is strongly affected by the thickness, and the electrical properties of the tab material. This model could be used to find appropriate tab dimensions to minimize the high rate tab temperatures.

The current collector potential profiles at the end of 5C discharge simulated by the linear and the full-distribution models for thermal condition case 1 are presented in Fig. 10(a) and (b), and the linear model still agrees very well with the full-distribution model. As shown in Fig. 10, the electrical potentials of current collectors change by 10–20 mV through the cell and tab sub-domains, and the potential gradients in the tabs are larger than that in the cell sub-domain due to the high planar current density in the tabs.

4. Conclusion

In this work, a multi-scale multi-dimensional thermal model for Li-ion cell was developed and a linear approximation was also proposed to simplify this model. The linear model is much more efficient than the full-distribution model in terms of the computation time. The linear model also maintains high accuracy in the predictions of most model variables except the two coupling variables which are directly approximated linearly to decouple the sub-domains, but this error does not affect the evaluation of other variables. Therefore, the linear model is an effective approach to study the distributed electrical and thermal behavior of an electrode plate pair in a Li-ion cell. In the future, this model will be extended to include multiple electrode plate pairs and model predictions will be further validated by experimental data.

Appendix A

The physical properties of the solution phase are shown in Equations (A1)–(A3). In these equations, the solution phase

concentration c_e is in mol m^{-3} and temperature T is in K. The diffusion coefficient of bulk electrolyte, $D_{e,\text{bulk}}$, is of the unit $m^2\ s^{-1}$.

$$D_{e,\text{bulk}} = 5.84\times10^{-7}\exp\left(-\frac{2870}{T}\right)\left(\frac{c_e}{1000}\right)^2 - 33.9\times10^{-7}\exp\left(-\frac{2920}{T}\right)\left(\frac{c_e}{1000}\right) + 129\times10^{-7}\exp\left(-\frac{3200}{T}\right) \quad \text{(A1)}$$

The electrical conductivity of bulk electrolyte, κ_{bulk}, is of the unit S m^{-1}.

$$\kappa_{\text{bulk}} = 3.45\exp\left(-\frac{798}{T}\right)\left(\frac{c_e}{1000}\right)^3 - 48.5\exp\left(-\frac{1080}{T}\right)\left(\frac{c_e}{1000}\right)^2 + 244\exp\left(-\frac{1440}{T}\right)\left(\frac{c_e}{1000}\right) \quad \text{(A2)}$$

The transference number of electrolyte, t^+, is dimensionless.

$$t^+ = 2.67\times10^{-4}\exp\left(\frac{833}{T}\right)\left(\frac{c_e}{1000}\right)^2 + 3.09\times10^{-3}\exp\left(\frac{653}{T}\right)\left(\frac{c_e}{1000}\right) + 0.517\exp\left(-\frac{49.6}{T}\right) \quad \text{(A3)}$$

The open circuit potentials of the negative and positive electrodes are shown in Equations (A4) and (A5), where U_n and U_p are in V.

$$\begin{aligned} U_n = {} & 0.124 + 1.5\exp(-70\,\theta_n) \\ & - 0.0351\ \tanh(12.0482\,\theta_n - 3.4458) \\ & - 0.0045\ \tanh(8.4034\,\theta_n - 7.5630) \\ & - 0.035\ \tanh(200\,\theta_n - 19.80) \\ & - 0.0147\ \tanh(29.4118\,\theta_n - 14.7059) \\ & - 0.102\ \tanh(7.0423\,\theta_n - 1.3662) \\ & - 0.022\ \tanh(60.9756\,\theta_n - 59.7561) \\ & - 0.011\ \tanh(44.2478\,\theta_n - 5.4867) \\ & - 0.0155\ \tanh(34.4828\,\theta_n - 3.6207) \end{aligned} \quad \text{(A4)}$$

$$\begin{aligned} U_p = {} & 1.638\,\theta_p^{10} - 2.222\,\theta_p^9 + 15.056\,\theta_p^8 - 23.488\,\theta_p^7 \\ & + 81.246\,\theta_p^6 - 344.566\,\theta_p^5 + 621.3475\,\theta_p^4 - 554.774\,\theta_p^3 \\ & + 264.427\,\theta_p^2 - 66.3691\,\theta_p + 11.8058 \\ & - 0.61386\ \exp\left(5.8201\,\theta_p^{136.4}\right) \end{aligned} \quad \text{(A5)}$$

References

[1] V. Srinivasan, C.Y. Wang, J. Electrochem. Soc. 150 (1) (2003) A98–A106.
[2] G.-H. Kim, A. Pesaran, R. Spotnitz, J. Power Sources. 170 (2) (2007) 476–489.
[3] S. Santhanagopalan, P. Ramadass, J. Zhang, J. Power Sources. 194 (1) (2009) 550–557.
[4] U.-S. Kim, C.-B. Shin, C.-S. Kim, J. Power Sources. 189 (1) (2009) 841–846.
[5] C.Y. Wang, V. Srinivasan, J. Power Sources. 110 (2) (2002) 364–376.
[6] R.E. Gerver, J.P. Meyers, J. Electrochem. Soc. 158 (7) (2011) A835–A843.
[7] G.-H. Kim, K. Smith, K.-J. Lee, S. Santhanagopalan, A. Pesaran, J. Electrochem. Soc. 158 (8) (2011) A955–A969.
[8] V. Ramadesigan, P.W.C. Northrop, S. De, S. Santhanagopalan, R.D. Braatz, V.R. Subramaniana, J. Electrochem. Soc. 159 (3) (2012) R31–R45.
[9] M. Doyle, T. Fuller, J. Newman, J. Electrochem. Soc. 140 (6) (1993) 1526.
[10] S. Santhanagopalan, Q. Guo, P. Ramadass, R.E. White, J. Power Sources. 156 (2) (2006) 620–628.
[11] K. Kumaresan, G. Sikha, R.E. White, J. Electrochem. Soc. 155 (2) (2008) A164–A171.
[12] K. Smith, C.-Y. Wang, J. Power Sources. 161 (1) (2006) 628–639.
[13] K.A. Smith, C.D. Rahn, C.-Y. Wang, Energ. Convers. Manage. 48 (2007) 2565–2578.
[14] V.R. Subramanian, V. Boovaragavan, V.D. Diwakar, Electrochem. Solid-State Lett. 10 (11) (2007) 255–A260.
[15] V. Ramadesigan, V. Boovaragavan, J.C. Pirkle, V.R. Subramaniana, J. Electrochem. Soc. 157 (7) (2010) A854–A860.
[16] P.W.C. Northrop, V. Ramadesigan, S. De, V.R. Subramanian, J. Electrochem. Soc. 158 (12) (2011) A1461–A1477.
[17] M. Guo, R.E. White, J. Power Sources. 198 (1) (2012) 322–328.

List of symbols

a_j: Specific surface area of electrode ($m^2\ m^{-3}$)
A_{Cell}: Area of the cell Sub-domain (m^2)
c_e: Concentration of Li in solution phase (mol m^{-3})
$\bar{c}_e$: Average electrolyte concentration (mol m^{-3})
C_P: Specific heat capacity ($J\ K^{-1}\ kg^{-1}$)
$c_{s,j}$: Concentration of lithium in the solid phase particles (mol m^{-3})
$c_{s,j,max}$: Maximum Li capacity in solid phase (mol m^{-3})
d: Distance between the two planar heat transfer surfaces (m)
$D_{2,eff}$: Effective diffusion coefficient of solution phase ($m^2\ s^{-1}$)
$D_{e,bulk}$: Diffusion coefficient in bulk solution phase ($m^2\ s^{-1}$)
$D_{s,j}$: The temperature-dependent particle diffusion coefficient ($m^2\ s^{-1}$)
$D_{s,j,ref}$: Reference particle diffusion coefficient ($m^2\ s^{-1}$)
$Ea_{di,j}$: Activation energy for particle diffusion ($J\ mol^{-1}$)
$Ea_{re,j}$: Activation energy for reaction ($J\ mol^{-1}$)
$f_{\pm}$: Activity coefficient of solution phase
F: The Faraday constant ($C\ mol^{-1}$)
h: Heat transfer coefficient for Newton's law of cooling ($W\ K^{-1}\ m^{-2}$)
i_1: Solid phase current density ($A\ m^{-2}$)
i_2: Solution phase current density ($A\ m^{-2}$)
$i_{app,j}$: Applied outward current density on the top of electrode tabs ($A\ m^{-2}$)
$i_{N,j}$: Current density through the coating/current-collector intersection ($A\ m^{-2}$)
i_N: Transverse current density ($A\ m^{-2}$)
$i_{x,j}$: Planar current density in X direction ($A\ m^{-2}$)
$i_{x,j}$: Planar current density in Y direction ($A\ m^{-2}$)
I_{app}: Total applied current on the electrode pair (A)
J_j: Rate of electrochemical reaction at the solid/solution surface ($mol\ m^{-2}\ s^{-1}$)
$k_{r,j}$: The Temperature-dependent reaction rate constant ($m^{2.5}\ mol^{-0.5}\ s^{-1}$)
$k_{r,j,ref}$: Reference reaction rate constant ($m^{2.5}\ mol^{-0.5}\ s^{-1}$)
k_{X-Y}: Planar thermal conductivity ($W\ K^{-1}\ m^{-1}$)
l_j: Thickness of electrode j or separator (m)
n: Unit normal vector pointing out of the boundary
q'_{rev}: Local reversible heat ($W\ m^{-3}$)
q'_{irrev}: Local irreversible heat ($W\ m^{-3}$)
Q: The total heat source ($W\ m^{-3}$)
Q_{ECh}: The electrochemical heat ($W\ m^{-3}$)
Q_H: Reaction enthalpy change throughout the porous electrode sub-domain ($W\ m^{-3}$)
$Q_{J,j}$: The Joule heat in the current collectors ($W\ m^{-3}$)
Q_{Trans}: Transversal heat transfer rate ($W\ m^{-3}$)
R: The universal gas constant ($J\ mol^{-1}\ K^{-1}$)
R_s: Radius of active material particles (m)
t^+: Transference number of electrolyte
T: Temperature (K)
T_{amb}: Ambient temperature (K)
T_{ref}: Reference temperature (K)
U_j: Open circuit potential of electrode (V)
W_E: Electrical work on the porous electrode sub-domain ($W\ m^{-3}$)
β_j: Bruggeman factor of electrode or separator
δ_j: Thickness of current collector j (m)
ε_e: Volume ratio factors of the porous electrode
$\varepsilon_{cc,j}$: Volume ratio factors of the current collector
ε_j: Porosity of electrode or separator
$\varepsilon_{s,j}$: Volume fraction of active material in the porous electrode
η_j: The electrode overpotential (V)
θ_j: Electrode state of charge
κ_{eff}: Ionic effective electrical conductivity of solution phase ($S\ m^{-1}$)
κ_{bulk}: Ionic electrical conductivity in bulk solution ($S\ m^{-1}$)
ρ: Density of electrode pair ($kg\ m^{-3}$)
σ_j: Electrical conductivity of pure active material ($S\ m^{-1}$)
$\sigma_{j,eff}$: Effective electrical conductivity of solid phase ($S\ m^{-1}$)
ϕ_1: Electrical potential of solid phase (V)
ϕ_2: Electrical potential of solution phase (V)
Φ_j: Electrical potential of current collector (V)
Ω_{Cell}: Symbol of the cell sub-domain in integral